Journal of CO_2 Utilization 28 (2018) 15–25

Contents lists available at ScienceDirect

Journal of CO_2 Utilization

journal homepage: www.elsevier.com/locate/jcou

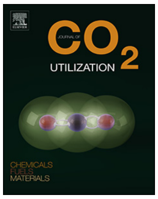

Enhanced photocatalytic CO_2 reduction activity of Z-scheme CdS/$BiVO_4$ nanocomposite with thinner $BiVO_4$ nanosheets

Zhi-He Wei, Yan-Fang Wang, Yan-Yang Li, Lin Zhang, Hong-Chang Yao*, Zhong-Jun Li*

College of Chemistry and Molecular Engineering, Zhengzhou University, Zhengzhou, 450001, China

ARTICLE INFO

Keywords:
Photocatalyst
CO_2 reduction
CdS/$BiVO_4$ composites
Z-scheme

ABSTRACT

Construction of Z-scheme photocatalysts has drawn much attention in the field of CO_2 reduction. However, research on photoreduction CO_2 for monoclinic bismuth vanadate (*m*-$BiVO_4$) is restricted due to its low conduction band potential and short electron diffusion lengths. To address the issues, we herein constructed a series of CdS/$BiVO_4$ nanocomposites by depositing CdS on the surface of $BiVO_4$ coupling with controlling the thickness of $BiVO_4$ nanosheets. The morphological, crystalline, band alignment and optical properties of the samples are investigated intensively. Photocatalytic performance is evaluated by measuring the ability of the photocatalysts to convert CO_2 into CO and hydrocarbon fuels, primarily CH_4. The composites exhibit more efficient photocatalytic activity than CdS and $BiVO_4$, and the yields of CH_4 and CO vary depending on the thickness of $BiVO_4$ substrate. The maximum yields of CH_4 and CO for CdS/$BiVO_4$ with 55–75 nm $BiVO_4$ are 2.98 and 1.31 μmol g^{-1} after 5 h irradiation, while those for its counterpart with 15–30 nm $BiVO_4$ attain 8.73 and 1.95 μmol g^{-1}, respectively. The enhanced photoactivity of the composites is attributed to the band structure and Z-scheme charge transfer mode. Besides, thinner $BiVO_4$ nanosheets are confirmed to be favorable for improving the photoreduction CO_2 efficiency due to shorter electron diffusion lengths.

1. Introduction

The inevitable increase in population and economic development has accelerated the fast depletion of fossil fuels and simultaneously, the rapid increase of atmospheric carbon dioxide (CO_2) concentration [1,2]. According to the prediction of the Intergovernmental Panel on Climate Change, the CO_2 content in the atmosphere would reach up to 590 ppm by 2100, and the global average temperature may rise by 1.9 °C, which will probably results in catastrophic consequences such as ice melting, sea level rising and climate changing [3]. Therefore, there is an urgent need to exploit renewable technologies that can reduce CO_2 emissions for the sustainable development of human society. Among various proposed strategies, solar photocatalytic conversion of CO_2 with H_2O into valuable chemicals, such as CO and hydrocarbon fuels, is considered as a promising way that not only addresses global warming but also partly satisfies renewable fuel demand [4,5]. Photocatalysts play a crucial role in the conversion process and hence, tremendous efforts have been devoted to the development of efficient catalysts in the past few decades, especially those with visible light response [6,7]. So far, the most notably visible-light-driven (VLD) metal oxides and sulfides including WO_3 [8], Bi_2WO_6 [9], $BiVO_4$ [10], and CdS [11] have been identified as promising photocatalysts for CO_2 reduction. However, their solar-to-fuel (STF) conversion efficiency is not impressive because it is difficult for single photocatalyst to meet all the stringent requirements for CO_2 reduction and water oxidation simultaneously. Therefore, various strategies, such as nanostructuralization, heterojunction formation and Z-scheme constructing, have been explored to improve the STF conversion efficiency [4,5,12].

As an important VLD photocatalyst, monoclinic bismuth vanadate (*m*-$BiVO_4$) has attracted intense scientific interest due to its proven high activity for solar water splitting and organic decomposition [13–15]. More attractively, *m*-$BiVO_4$ has appropriate band edges, which makes it suitable for water oxidation coupled with CO_2 reduction [16]. It has been reported that *m*-$BiVO_4$ could be used as photocatalyst for the reduction of CO_2 into ethanol [10]. Unfortunately, $BiVO_4$ suffers from poor electron transport [17,18] and extremely low carrier mobility ($\sim 10^{-2}$ cm^2 V^{-1} s^{-1}) [19], resulting in significant recombination of electron-hole pairs and poor charge-carrier transportation. To address these problems, researchers have focused much research on the design of nanostructured materials [14]. In this regard, two dimensional (2D) nanosheets are particularly promising in improving charge separation as the photogenerated electrons and holes will travel shorter distances to reach both end interfaces of nanosheets. Recently, Mao et al. synthesized lamellar $BiVO_4$ by a surfactant-assisted hydrothermal method

---

* Corresponding authors.
E-mail addresses: yaohongchang@zzu.edu.cn, hchyao111@163.com (H.-C. Yao), lizhongjun@zzu.edu.cn (Z.-J. Li).

https://doi.org/10.1016/j.jcou.2018.09.008
Received 16 June 2018; Received in revised form 1 September 2018; Accepted 8 September 2018

and used it as a photocatalyst for CO_2 reduction [20]. The results show that the lamellar material with the thickness in the range of 0.08–0.12 μm exhibited a selective methanol production under visible light irradiation. It should be noted that the reported electron diffusion length in undoped $BiVO_4$ is as low as 10 nm [21]. Therefore, it is highly desirable to control the thickness of the synthesized $BiVO_4$ catalyst in order to achieve higher carrier separation efficiency.

Apart from nanostructuring, other strategies have also been explored to enhance the charge separation of $BiVO_4$–based catalysts [14]. Of particular interest is the design of staggered heterojunction configuration (type II) by coupling $BiVO_4$ with a suitable semiconductor that has properly aligned band structures [22]. Formation of such heterojunctions results in the movements of photoinduced electrons and holes at the interface in opposite directions, improving both spatial separation and collection efficiency of the photo-generated charges. Successful heterojunction formation of $BiVO_4$ has been reported with WO_3 [23], Bi_2O_3 [24], and Bi_2S_3 [25]. Regretfully, such charge transfer mode is unfavorable for water oxidation and CO_2 reduction because it results in lower oxidation and reduction potentials. By contrast, hterostructured Z-scheme photocatalysts, in which the carrier movements directly quench the weaker oxidative holes and reductive electrons, are beneficial for water oxidation and CO_2 reduction [12]. Representative $BiVO_4$–based Z-scheme systems have been reported for different applications, including water splitting, hydrogen production and photodegradation [26,27]. Recently, our group synthesized direct Z-scheme α-Fe_2O_3/Cu_2O heterostructures [28] and indirect Z-scheme BiOI/g-C_3N_4 photocatalysts [29], and the photoreduction CO_2 activities of these materials were investigated comprehensively under visible light irradiation. However, $BiVO_4$–based Z-scheme systems for CO_2 reduction, as far as we know, have been reported scarcely up to now [30].

CdS is a VLD semiconductor with narrow band gap (2.4 eV), which is suitable for the application in photochemical catalysis [31]. Particularly, CdS could be used for CO_2 reduction owing to its appropriate conduction band (CB) edge of –0.6 eV (*vs.* NHE) [32,33]. Unfortunately, severe light corrosion phenomenon of CdS usually resulted in a decrease of the photo-stability, greatly limiting its application in photoreduction CO_2. On the other hand, CdS suffers from the drawback of high recombination of photogenerated electron-hole pairs [34]. Tremendous efforts have thus been devoted to suppressing the recombination of electron–hole pairs and the photocorrosion of CdS. Among the methods that increase the photo-stability and charge separation efficiency, constructing Z-scheme heterostructures is demonstrated to be an effective one, probably because of the spatial separation of photogenerated charges and the holes of CdS quenched by photoinduced electrons of another semiconductor [35].

In the present study, we synthesized a series of heterostructured CdS/$BiVO_4$ composites by depositing different amounts of CdS on the surface of $BiVO_4$ nanosheets coupling with adjusting the thickness of $BiVO_4$. The phase, elemental composition and morphology of the obtained materials were characterized by X-ray diffraction (XRD), X-ray photoelectron spectroscopy (XPS), scanning electron microscopy (SEM) and high resolution transmission electron microscopy (HRTEM). The band structure for the typical CdS/$BiVO_4$ composite was characterized by UV–vis reflectance spectroscopy and X-ray/ultraviolet photoelectron spectroscopy. The photoreduction CO_2 activities of the prepared samples were evaluated in the presence of water vapor under simulated visible light. The results show that CdS/$BiVO_4$ nanocomposites exhibit higher photocatalytic CO_2 reduction activity than pure $BiVO_4$ and CdS and the yields of products CO and CH_4 are changed with the loading content of CdS in the composites. Furthermore, it is proved that the photocatalytic activity of the composites is closely related to the thickness of $BiVO_4$ substrate. The enhancement of photocatalytic activity of the optimal CdS/$BiVO_4$ nanocomposite is attributed to the synergistic effect of forming Z-scheme herterojunction and reducing thickness of $BiVO_4$. The mechanism of photocatalytic CO_2 reduction is further proposed.

2. Experimental

2.1. Materials

All the reagents used, including bismuth nitrate pentahydrate ($Bi(NO_3)_3{\cdot}5H_2O$), ammonium metavanadate (NH_4VO_3), thiourea (CN_2H_4S), cadmium acetate ($Cd(CH_3COO)_2{\cdot}2H_2O$), and sodium hydroxide (NaOH), were obtained from Sinopharm Chemical Reagent Co., Ltd. (Shanghai, China) and used as received without further purification.

2.2. Synthesis

2.2.1. Preparation of $BiVO_4$ nanosheets

$BiVO_4$ nanosheets were synthesized by the hydrothermal method. 2 mmol (0.970 g) of $Bi(NO_3)_3{\cdot}5H_2O$ and 1.5 mmol (0.522 g) of $C_{18}H_{29}NaO_3S$ (SDBS) were dissolved in 20 mL of HNO_3 (4 M) to form solution A, while 2 mmol (0.234 g) of NH_4VO_3 were dissolved in 20 mL of NaOH solution (2 M) to form solution B. Then solution B was added into solution A dropwise under magnetic stirring at room temperature. After 0.5 h, the pH value of the mixed solution was adjusted to 2.5 and 6.5, respectively, with NaOH solution (2 M). The resulting solutions were sealed in Teflon-lined stainless steel autoclave and transferred to the oven at 160 °C for 2 h. The obtained products were washed by distilled water and absolute alcohol for several times, and then dried at 70 °C overnight. The prepared powders are named on the basis of preparation condition as **I-BV** (pH 2.5) and **II-BV** (pH 6.5), respectively.

2.2.2. Preparation of CdS/$BiVO_4$ composites

In a typical experiment, CdS/$BiVO_4$ composites were synthesized by the modified method reported previously [36]. $Cd(CH_3COO)_2{\cdot}2H_2O$ with different moles was dissolved in 50 mL of deionized water to form solution C. A fixed amount of the as-prepared $BiVO_4$ powders (0.25 mmol, 0.081 g) were added into the solution C, and the mixture was treated ultrasonically for 0.5 h. Then 10 mL thiourea solution with different concentration (Table S1) was dipped into the above mixture with vigorous stirring for 20 min. After the mixture was heated at 90 °C for 2.5 h, the obtained products were washed with distilled water and absolute alcohol, and then dried at 70 °C for 12 h. The scheme diagram of the preparation process of CdS/$BiVO_4$ composites and the description of the growth mechanism are presented in Fig. S1. The prepared powders were labeled as **I-BC-*x*** and **II-BC-*x***, ***x*** represnts 3, 4, 5 and 6 according to the Cd/Bi molar ratio of synthesis materials. To verify the real CdS percentage in the final CdS/$BiVO_4$ composites, energy dispersive spectroscopy (EDS) accompanying elemental and chemical analysis was conducted and the results are shown in Table S2. From the results of EDS mapping analysis, the real weight percentage of CdS in the **I-BC-*x*** is 12.4, 23.7, 31.3, and 47.2%, respectively, while that of **II-BC-*x*** is 10.6, 21.5, 30.7 and 45.4%, respectively.

2.3. Characterization

The crystal phase of the samples was characterized on X–ray diffractometer (XRD, PANalytical X' pert PRO). The morphology and composition were recorded by Field emission scanning electron microscopy (FESEM, Sigma 500) equipped with an energy-dispersive X-ray spectroscopy analyzer (EDS) and transmission electron microscopy (TEM, TECNAI G^2 F20-S-TWIN). Moreover, high-resolution transmission electron microscopy (HRTEM) was employed. UV–vis diffuse reflectance spectra (DRS) were determined by a scan UV–vis spectrometer (Cary 5000) with integrating sphere detector. Chemical components and valence states were analyzed using X-ray photoelectron spectroscopy (XPS, PerkinElmer PHI 5300). Brunauer-Emmet-Teller (BET) surface area was measured with a Quantachrome Autosorb-IQ2